Neuron, Volume *58*

Supplemental Data

Attention Modulates Earliest Responses in the Primary Auditory and Visual Cortices

Vahe Poghosyan and Andreas A. Ioannides

Data recording and analysis

MEG was recorded using a 151 gradiometer whole-head system (CTF Systems Inc., Canada) at a sampling rate of 2500 Hz and bandpass of 0-800 Hz. In synchrony with the MEG, vertical and horizontal electrooculogram (EOG) and electrocardiogram (ECG) were recorded. Electrodes for the horizontal EOG (hEOG) were placed symmetrically on the skin at the outer ocular canthus of each eye, aligned horizontally with the pupil. Vertical EOG was recorded with electrodes placed above and below the left orbit and aligned vertically with the pupil. hEOG was used for verifying the fixation, while vertical EOG was effective in detecting the blinks.

Before the experiment, for each subject an eye movement calibration procedure was conducted to determine the voltage produced at the hEOG electrodes by eye movements of a known size. This calibration run was recorded under ambient light conditions identical to the experimental one. During the run, five white dots were presented to the subject, one at the fixation and two in each (left and right) lower quadrant of visual field at 5° and 10° eccentricities along the 45° diagonals. By moving only the eyes, subjects had to follow a black dot, which started at the fixation, then moved to one of the white dots, stayed there for one second and then moved back to the fixation. hEOG amplitude at fixation was effectively 0, while at 5° and 10° it was ~20 μV and ~40 μV respectively. Analysis of the hEOG signals recorded for individual subjects during the calibration runs confirmed that at these

eccentricities (< 10°) the EOG voltage change is approximately linearly related to the angle of eye movement (Shackel, 1967). On the basis of this calibration procedure, we estimated the average eye movements over a range of latencies by averaging separately the positive and negative EOG deflections. In this way, we determined that the average eye movement in each run was less than 0.3° and that in the interval from -100 to 100 ms relative to stimulus onset there were no eye movements exceeding the 1° threshold (hEOG of ~4 μV). Critically, statistical analysis revealed no differences in the amplitude of hEOG signals recorded in the runs where attention was directed to left vs. right visual field ($t = 0.15$, $P > 0.86$). The average voltage produced by leftwards and rightwards eye movements was 0.74 and -0.75 μV in the attend left and 0.84 and -0.86 μV in the attend right runs respectively.

The subject's head location relative to MEG sensors was recorded at the beginning and end of each run, using head localization coils attached to the subject's head. Average head movement of each subject during a run was around 1-2 mm. Runs in which movement exceeded 4 mm were repeated. Coregistration of the MEG sensors with the individual high-resolution anatomical MRIs was accomplished using a procedure described in Poghosyan and Ioannides (2007), which provides a coregistration accuracy of 1 mm (Hironaga and Ioannides, 2002).

Offline, the MEG signals were converted to a 3rd order synthetic gradient and high-pass filtered at 1 Hz. Independent component analysis in conjunction with vertical EOG and ECG data was used to remove the eye blink and cardiac artifacts respectively. The processed MEG signals were averaged for each run and stimulus separately, with respect to the stimulus onset (-100 to 200 ms).

The subject's head location relative to the sensors is slightly different in each run. Since different attentional conditions were blocked in different runs, one must allow for differences in the MEG signal that might be entirely due to differences in the location of the

sensors relative to the head in different attentional conditions. To address this point standardized values of MEG signals were used to compare signals in “attended” vs. “ignored” runs. For this purpose, signals from each sensor in each run were z-transformed based on the average and standard deviation across MEG signals from all sensors in that run. We compared signals from sensors with strongest peak amplitude in the given latency range (see below) in each attentional condition, rather than signals from the same sensor, since they are more likely to reflect the same neural activity patterns. We note however that in most cases the same sensor was selected for “attended” and “ignored” runs and in the other few cases one of the nearby sensors was selected. In addition, in the few cases where different sensors were selected, further comparisons using the signals from the same sensor did not alter the main findings.

Source analysis of averaged MEG signals (not standardized) for each subject was performed using MFT followed by SPM. We stress that the concerns raised in the last paragraph do not affect the MFT analysis, which automatically compensates for the change in the relative position of sensors and the subject head. All MFT computations of the current density are performed in the anatomical space defined by the MRI of each subject. The full details of the MFT/SPM source analysis can be found elsewhere (Moradi et al., 2003;Poghosyan et al., 2005;Poghosyan and Ioannides, 2007). A brief summary of the basic concepts underlying MFT is given below, in the subsection “Summary of MFT”. Prior to SPM, current density vectors (MFT solutions) were integrated over 2.4 ms (6 timeslices) successive windows, and the moduli of the resulting integrated current density vectors were used for the SPM analysis. A basic distribution for each run, stimulus category and presentation side consisted of 12 elements, the moduli of the integrated current density vectors over four consecutive windows for each of the three stimuli of the same category (e.g. neutral, happy and angry faces). SPM was performed in two ways. First, to identify the

sensory-evoked activations, for each stimulus category (low frequency tones, high frequency tones, checkerboards or faces) presented in each side (left or right), distributions were formed by putting together the basic distributions from the two non-spatial attention runs of the sensory modality, different from that of the presented stimulus category's. Thus, in this case each distribution contained 24 elements (4 windows × 3 stimuli × 2 runs). High-resolution statistical maps were then constructed by comparing such distributions, drawn from the post- and prestimulus periods of MFT solutions, using Student's t-test. Second, to identify the attention related activations, for each stimulus category presented in each side, basic distributions, drawn from the same latencies of the two sensory modality specific spatial attention runs were compared. After each statistical comparison, the basic distribution was moved forward by two integration windows (4.8 ms) until the end of the period (200 ms poststimulus). In the first case, only the poststimulus distribution was moved forward, the prestimulus distribution was kept the same.

The earliest statistically significant ($P < 0.005$) activation was identified from each resultant high-resolution statistical map. Centroids of these activations were then designated as centers of spherical ROIs with a radius of 7 mm. RACs for each ROI were generated from the MFT solutions derived from the modality specific spatial attention runs, using steps described in Poghosyan and Ioannides (2007). RACs were then averaged according to stimulus category and across subjects to produce grand-averaged RACs. Solely for display purposes, grand-averaged RACs were smoothed using a 10 ms running window.

Amplitudes and latencies of peaks in the intervals of 25-55 and 60-120 ms for auditory, and 50-90 and 90-150 ms for visual stimuli were extracted from individual RACs and MEG signals recorded in the spatial attention runs. Separate ANOVA analysis was performed for each sensory modality and time interval, with attentional condition (same stimulus when attended and ignored), stimulus category (visual: checkerboards and faces;

auditory: high and low frequency tones) and presentation side (left and right) as fixed and subject (five subjects) as random factors. For RACs ROI was used as an additional fixed factor. Two ROIs were used for visual (left and right V1), and four ROIs for auditory (left and right A1, each defined for low and high frequency tones) stimuli.

Hit rates and reaction times were also analyzed using ANOVA. In this case task's modality (auditory and visual) and required type of attention (spatial and non-spatial) were used as fixed factors. In addition, for spatial attention runs, dependence of the performance on attention's direction (left or right side) was tested using presentation side as a fixed factor. In all cases, SPSS (SPSS Inc., USA) statistical software package was used for ANOVA.

ECD source analysis

To increase signal-to-noise ratio for the ECD source analysis, MEG signals recorded in the spatial attention runs were averaged over all stimuli of the same sensory modality, separately for each subject, run and presentation side. Dipolar sources of MEG signals were estimated using Brain Electrical Source Analysis (BESA, MEGIS Software GmbH, Germany) software. Before applying the dipole fit, averaged MEG signals were low-pass filtered at 80 Hz (Martinez et al., 1999). Two modeling approaches were taken. In both cases the minimal GOF was set to 80%. GOF has been defined as the proportion of the measured signal variance accounted for by the model. In the first approach ECD analysis was guided by the results of MFT/SPM source analysis (MFT/SPM guided fit). In this case, prior to fitting, dipoles were placed at the locations of modality specific ROIs, identified for the corresponding presentation side. For visual stimuli, dipole was placed at the center of V1 ROI, whereas for auditory stimuli, it was placed at the midpoint of putative A1 ROIs, which were defined in response to low and high frequency tones. During the fits, locations of these dipoles were fixed, but orientations were allowed to vary. Another dipole, with free location

and orientation, was seeded in the contralateral superior temporal or lateral occipital cortex for auditory and visual stimuli respectively. Fifteen-millisecond intervals around the peak latencies of grand-averaged RACs were selected for dipole fits. Intervals of 30-45 and 65-80 ms were used for auditory and visual stimuli respectively. The same intervals were used in all subjects. For auditory responses in the specified interval, two-dipole model provided adequate GOF in all subjects. Visually evoked responses required an extra dipole to satisfactorily fit the data. The additional dipole was seeded in the contralateral occipital cortex and its location and orientation were set free. Separate dipole fits were carried out for the runs where each presentation side was attended and ignored. After the fit, source waveforms of fixed dipoles were extracted from different runs and compared. The source waveforms were calculated by multiplying the inverse lead field matrix of the dipoles by the measured MEG signals. This procedure decomposes the measured signals into separate contributions from the source waveforms of each dipole in the model. Though the dipoles in our study were fit in separate 15 ms intervals, the source waveforms of each dipole are generated for the whole time period (-100 to 200 ms).

In the second modeling approach we used the same procedures as the ones reported in earlier studies of visual spatial attention ("unguided" dipole fit) (Di Russo et al., 2003;Martinez et al., 2001;Noesselt et al., 2002). Only the data, obtained in the visual spatial attention runs were analyzed. At first, averaged MEG signals of the runs where the stimulated visual field was ignored, were fitted in the 50-65 ms interval, with a single dipole, which, prior to fit, was seeded around the corresponding V1 ROI. Then, while keeping the first dipole active, the signals in the 65-80 ms interval were fitted either with one dipole, seeded in the contralateral occipital cortex or with a pair of mirror symmetric dipoles, seeded in the occipital cortex bilaterally. Both fits for the second interval revealed very similar results. The dipole models, obtained for each simulated visual field from its ignored run, provided

adequate GOF in the attended run also. Source waveforms of all dipoles were extracted from both runs and compared.

To make the results of MFT/SPM guided and the unguided dipole fits more comparable, an additional MFT/SPM guided dipole fit was performed using a procedure more similar to the one used in the unguided fit. The data from the visual spatial attention runs, where the stimulated visual field was ignored were calculated over the same time interval as in the unguided fit (50-65 ms). In five out of ten cases (5 subjects × 2 hemispheres), the one dipole fixed at the V1 location determined from the MFT/SPM analysis, failed to fit the data with 80% GOF (in most cases it was ~70%). Therefore, the second dipole with free location was added to the model. The resultant two dipole models, over the 50-65 ms interval, provided adequate GOF in both spatial attention runs for each stimulated visual field, whether it was ignored or attended. The most representative results are shown in Supplemental Figure 1.

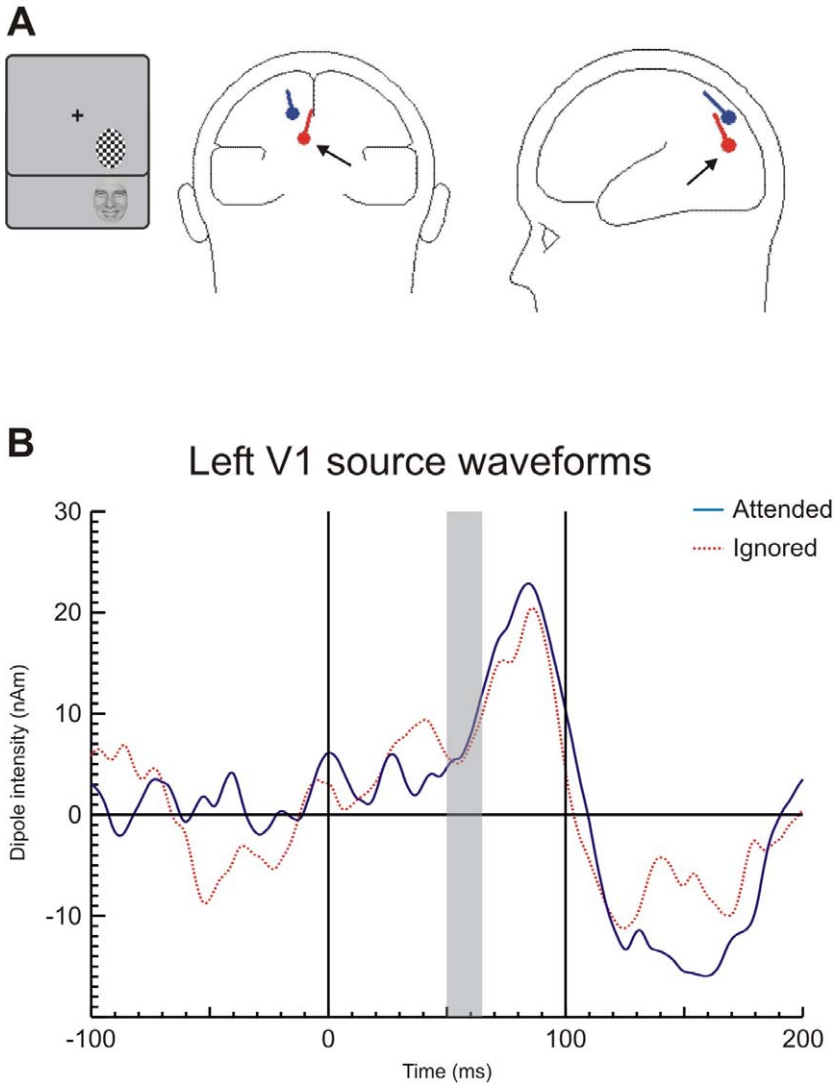

Supplemental Figure 1. Dipole modeling of MEG signal sources (MFT/SPM guided; representative examples from one subject). (A) Locations of dipoles for right visual field stimulations shown on coronal (left) and sagittal (right) views of the head scheme. Prior to fitting, location of one of the dipoles (red dipole, pointed by an arrow) was fixed according to ROIs identified by MFT/SPM source analysis. Two dipoles provided adequate GOF in the 50-65 ms interval (gray interval in (B)). (B) Source waveforms of fixed V1 dipole depicted in red and pointed by arrows in (A). Waveforms of dipoles in the runs where the stimulated visual field was attended (solid blue) and ignored (dotted red) are overplotted.

Summary of MFT

MFT is a non-linear method for solving the biomagnetic inverse problem. It provides a three-dimensional distribution of the primary currents throughout a predefined source space (in practice the entire brain).

The primary current distribution $\vec{j}(\vec{r})$ inside the source space *S* relates to the magnetic field b_i measured at i^{th} MEG sensor in terms of the lead field $\vec{\varphi}_i(\vec{r})$ for that sensor:

$$b_i = \int_S \vec{\varphi}_i(\vec{r}) \bullet \vec{j}(\vec{r}) d\vec{r}\,, \qquad i = (1, \ldots, N) \tag{1}$$

The lead field $\vec{\varphi}_i(\vec{r})$ is a vector function that describes the sensitivity distribution of the i^{th} sensor and is completely determined by the geometric properties of the measurement coil set and the conductivity details of the biological medium. The task is to estimate $\vec{j}(\vec{r})$ given the *N* measurements b_i. The unknown current density $\vec{j}(\vec{r})$ can be expressed as:

$$\vec{j}(\vec{r}) = \sum_{k=1}^{N} A_k \vec{\varphi}_k(\vec{r}) w(\vec{r}, |j(\vec{r})|) \tag{2}$$

where $w(\vec{r}, |j(\vec{r})|)$ is the *a priori* probability weight function, which in general can be a function of the source position and the unknown current source itself and A_k are scalar expansion coefficients, which must be determined together with $\vec{j}(\vec{r})$. By combining equations (1) and (2) we obtain a set of equations ($b_i = \sum_{k=1}^{N} A_k \int_S \vec{\varphi}_i(\vec{r}) \bullet \vec{\varphi}_k(\vec{r}) w(\vec{r}, |j(\vec{r})|) d\vec{r}$, i = 1, … , *N*), where from A_k and hence $\vec{j}(\vec{r})$ (equation (2)) can be determined, provided the form of the weight function $w(\vec{r}, |j(\vec{r})|)$ is fixed. Distributed source localization methods can be distinguished according to how they deal with the weight function. In its generalized form

(*generalized* MFT) MFT represents a family of algorithms, where the weight function $w(\vec{r},|j(\vec{r})|)$ is expressed as: $w(\vec{r},|j(\vec{r})|)=|j(\vec{r})|^{p+1}w(\vec{r})$. Different values of *p* lead to different methods, as is shown on the diagram below:

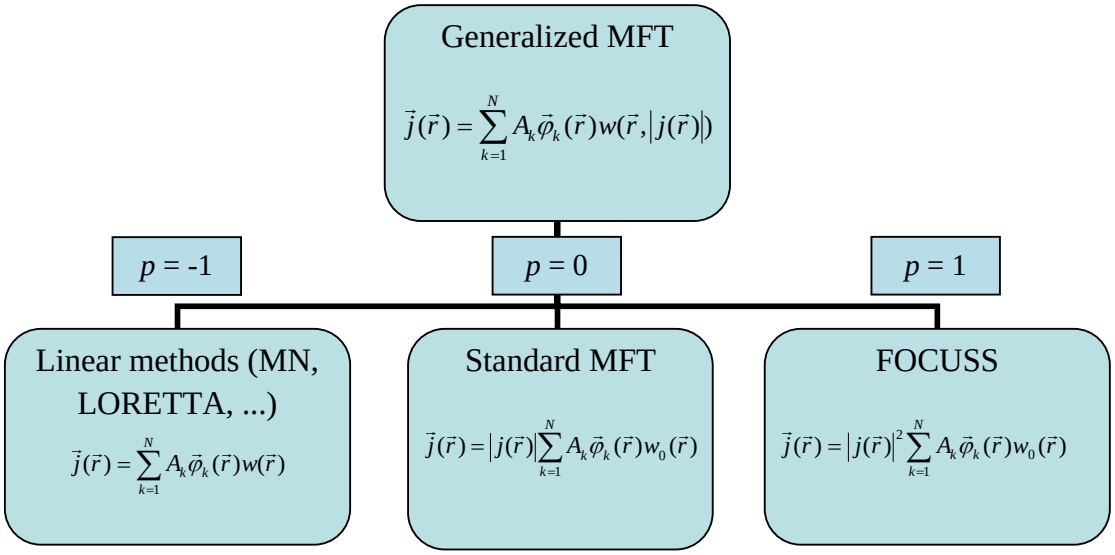

p = -1. The methods in this family presuppose that both direction *and strength* of current source distributions can be expressed in a single linear expansion in the lead fields. This assumption leads to linear methods (minimum norm (MN), weighted MN, LORETTA and spatial filtering methods), which are computationally easy to apply, but do not fully exploit the information in the measured MEG signals and over-rely on the raw lead fields. This is reflected in the blurred nature of their solutions.

p = 0. The *standard* MFT has been used in all our studies. It relies less on the raw lead fields and makes more use of the measured data. Specifically, it has a lesser assumption than the linear methods, in that in the standard MFT *only* the direction of the current distribution is expressed by a linear expansion in lead fields, as can be readily seen by dividing both sides of

the expression for $\vec{j}(\vec{r})$ by the $|j(\vec{r})|$. The strength of the source currents is determined more explicitly from the MEG signal itself by solving a highly non-linear system of equations for each timeslice of data. Simulation analysis (Ioannides et al., 1990) and theory (Taylor et al., 1999) show that standard MFT ($p = 0$) satisfies best the underlying physics and has the expected properties for localized distributed sources.

$p = 1$: The FOCUSS algorithms (corrected for gauge invariance) emphasizes the strong features in the signal and does not use the fine detail provided by the data. Its solutions are very focal; the strong current sources are accurately identified, whereas the weaker ones are suppressed.

Reference List

Di Russo,F., Martinez,A., and Hillyard,S.A. (2003). Source analysis of event-related cortical activity during visuo-spatial attention. Cereb.Cortex *13*, 486-499.

Hironaga,N. and Ioannides,A.A. (2002). Accurate co-registration for MEG reconstructions. In Proceedings of the 13th International Conference on Biomagnetism, H. Nowak, J. Haueisen, F. Giessler, and R. Huonker, eds. (Berlin: VDE Verlag), pp. 931-933.

Ioannides,A.A., Bolton,J.P.R., and Clarke,C.J.S. (1990). Continuous probabilistic solutions to the biomagnetic inverse problem. Inverse Problem *6*, 523-542.

Martinez,A., Anllo-Vento,L., Sereno,M.I., Frank,L.R., Buxton,R.B., Dubowitz,D.J., Wong,E.C., Hinrichs,H., Heinze,H.J., and Hillyard,S.A. (1999). Involvement of striate and extrastriate visual cortical areas in spatial attention. Nat.Neurosci. *2*, 364-369.

Martinez,A., Di Russo,F., Anllo-Vento,L., Sereno,M.I., Buxton,R.B., and Hillyard,S.A. (2001). Putting spatial attention on the map: timing and localization of stimulus selection processes in striate and extrastriate visual areas. Vision Res. *41*, 1437-1457.

Moradi,F., Liu,L.C., Cheng,K., Waggoner,R.A., Tanaka,K., and Ioannides,A.A. (2003). Consistent and precise localization of brain activity in human primary visual cortex by MEG and fMRI. Neuroimage. *18*, 595-609.

Noesselt,T., Hillyard,S.A., Woldorff,M.G., Schoenfeld,A., Hagner,T., Jancke,L., Tempelmann,C., Hinrichs,H., and Heinze,H.J. (2002). Delayed striate cortical activation during spatial attention. Neuron *35*, 575-587.

Poghosyan,V. and Ioannides,A.A. (2007). Precise mapping of early visual responses in space and time. Neuroimage *35*, 759-770.

Poghosyan,V., Shibata,T., and Ioannides,A.A. (2005). Effects of attention and arousal on early responses in striate cortex. European Journal of Neuroscience *22*, 225-234.

Shackel,B. (1967). Eye movement recording by electro-oculography. In A manual of psychophysical methods, P. H. Venables and I. Martin, eds. (Amsterdam: North-Holland), pp. 299-334.

Taylor,J.G., Ioannides,A.A., and Mueller-Gaertner,H.W. (1999). Mathematical analysis of lead field expansions. IEEE Trans.Med.Imaging *18*, 151-163.